Altimetric Parameter Estimation in Long Coherent Processing by Airborne Delay/Doppler Altimetry Based on Bayesian Learning

Cheng Fang, Ming Sun, Bo Huang, Fangheng Guan, Honghao Zhou, Xianhua Liao, and Lei Yang, *Member, IEEE*

***Abstract*—The along-track resolution of conventional airborne synthetic aperture radar altimetry (SARAL), where the coherent processing interval (CPI) is the burst length, is not a full resolution due to beam limited. For a fully focused radar altimeter image, a novel airborne SARAL processing algorithm based on a long CPI is proposed in this article. The long CPI is capable of achieving higher azimuthal resolution than that in the conventional altimeter with limited number of pulses. To conquer the problem of atmosphere turbulence and in accordance of motion deviation of the airborne platform, a subaperture phase gradient autofocusing framework is introduced to alleviate nonsystematic phase errors (NsPE). In this framework, NsPE is estimated and compensated in along-track so that a fully focused delayed Doppler map (DDM) can be guaranteed. Finally, the height parameter estimation is performed to the 1-D altimeter echoes after multilooking processing of DDM to improve the estimation accuracy. Given that the conventional retracking algorithm is sensitive to noise, which may degrade the estimation accuracy, a flexible Bayesian method is designed in a hierarchical manner for the SARAL retracking. The SARAL raw data are utilized in the experiment. The results of image entropy and RMSE demonstrate the effectiveness and superiority of the proposed algorithm both qualitatively and quantitatively.**

***Index Terms*—Coherent processing interval (CPI), hierarchical Bayesian learning, phase gradient autofocusing (PGA), synthetic aperture radar altimeter (SARAL).**

I. Introduction

RADAR altimeter usually transmits wide-band pulses to the nadir point and receives echoes in a pulse group (or burst). In general, the satellite/airborne radar altimeter performs in synthetic aperture mode to improve the accuracy of the altimetric parameter. Taking advantages of delay correction processing with orbit parameters, the ground elevation can be obtained by comparing with the earth reference ellipsoid. However, the conventional radar altimeters use the echo delay within the pulse-limit footprint to estimate minimum radar range [1]. Most of the radiated power falls outside the pulse limit footprint, which cannot be used for height estimation. A large part of the radiated power is wasted and the measurement accuracy is limited. Therefore, the delayed Doppler altimeter (DDA) is proposed and developed [1].

DDA, which is also called synthetic aperture radar altimeter (SARAL), is named because the processed 2-D echoes are in the domain of delay cross track and Doppler along-track [2]. Compared with the conventional radar altimetry, the resolution of SARAL is improved by an order of magnitude by means of the phase delay compensation cross-track and nonfocused multilooking coherent processing along-track on the principle of synthetic aperture imagery. Therefore, SARAL is widely used in hydrology and sea ice exploration [3], [4].

Conventional radar altimeters transmit and receive monopulse, whose coherent pulse interval (CPI) is burst length [5], [6]. The along-track resolution of altimeter depends on the number of the pulses in transmitted burst, where the CPI along-track is the burst period. To satisfy high resolution requirements of airborne radar altimeter, long CPI processing is introduced to obtain more target information than conventional ones. Specifically, by extending the conventional burst interval to the synthetic aperture period, the number of received pulses in the long CPI is accordingly increased, and rich height information is consequently obtained. Thus, the height measurement accuracy can be accordingly improved. However, due to the long CPI processing, motion errors are produced to the airborne SARAL, whose platform is susceptible to the atmosphere turbulence. Compared with the range migration caused by predictable changes in the relative distance between the radar and the target, the phase error due to the unknown motion of the platform is usually called nonsystematic phase error (NsPE) [7], [8]. Consequently, it is necessary but challenging to correct the NsPE [7], [8].

To solve the problem of motion errors from the airborne platform, algorithms dealing with NsPE are taken into consideration. Generally, there are two classical algorithms to dealing with nonsystematic errors: the phase gradient autofocusing (PGA) algorithm [9], [10] and the minimum entropy auto-focusing (MEA) [11], [12] algorithm. The MEA algorithm realizes phase error correction involve iteratively calculating and minimizing

Manuscript received 9 June 2023; revised 16 August 2023; accepted 28 August 2023. Date of publication 5 September 2023; date of current version 13 September 2023. This work was supported in part by National Natural Science Foundation of China under Grant 62271487 and in part by College Basic Research Funds under Grant 3122023PY07. *(Corresponding author: Bo Huang.)*

Cheng Fang, Ming Sun, Fangheng Guan, Honghao Zhou, Xianhua Liao, and Lei Yang are with the Tianjin Key Lab for Advanced Signal Processing, Civil Aviation University of China, Tianjin 300300, China (e-mail: cfang@cauc.edu.cn; sunming_0620@163.com; 2021021054@cauc.edu.cn; 13956195498@163.com; xhliao1@163.com; yanglei840626@163.com).

Bo Huang is with the Institute of Electronics Engineering, China Academy of Engineering Physics, Mianyang 621900, China (e-mail: vick123y@163.com).

Digital Object Identifier 10.1109/JSTARS.2023.3311913

the image entropy objective function. While in PGA, the NsPE is calculated through integral step. Then, the echo to be corrected is multiplied by the compensation phase term and the error correction procedure is achieved. Numerous practices prove that the PGA is a very stable phase correction algorithm, which obtains the gradient of the echo phase error through the phase gradient estimation. PGA performs rather prominent and stable properties compared with MEA. Nevertheless, in practical engineering, long CPI means large number of pulses carrying plenty height information, which may bring great burden to hardware data processing. Based on this, subaperture combined with PGA is designed to divide large data into several data slices so that a fully focused delayed Doppler map (DDM) can be obtained, which represents the altimeter delay in range and different Doppler positions.

Next, by along-track multilooking processing, 1-D altimeter echoes can be obtained. Halimi et al. [13] demonstrated that 1-D delayed echoes follow a three-term convolution model or Brown model, which establishes an analytical relationship between altimeter echoes and altimetry parameters. Therefore, various retracking algorithms based on the Brown model have been proposed for altimetry parameter estimation. The conventional altimetry parameter estimation algorithm is the least squares (LS) algorithm [13], [14]. Although LS is efficient, it is very susceptible to noise.

In this article, the long CPI is utilized so that fully focused DDM of radar altimeter can be obtained. PGA compensation under subaperture framework is proposed to alleviate motion errors caused by long CPI. Aiming at improving the accuracy of altimeter parameter estimation for up-and-down terrain, a flexible Bayesian learning algorithm is proposed, where the prior is modeled as a generalized Gaussian distribution (GGD). To solve the problem of the nonconjugation between prior and likelihood, hierarchical Bayesian combined with Hamiltonian Monte Carlo (HMC) sampler is designed to obtain closed-form solutions of the height parameter posterior. The airborne raw SARAL data are employed to validate the effectiveness of the proposed algorithm. Also, comparisons with the conventions examine the superiority of the proposed algorithm.

The organization of this article is as follows: Section II describes the SARAL geometry and echo model. The long coherent processing method is discussed in Section III, where the 2-D delay/Doppler echo mathematical model is derived, and the NsPE correction is illustrated. The Bayesian altimetry parameter retracking is given in Section IV. In Section V, the processing procedure of the proposed algorithm is demonstrated. Experiments are conducted and analyzed in Section VI. Discussions and conclusions are given and drawn in Sections VII and VIII, respectively.

II. SARAL Geometry and Echo Model

The airborne SARAL geometry is depicted in Fig. 1, where the SARAL flies with the speed of v along the direction of Y, which is called along-track. It transmits linear frequency modulation (LFM) pulses to the nadir vertically, and echoes are received for processing to obtain the ground height. The Cartesian coordinate

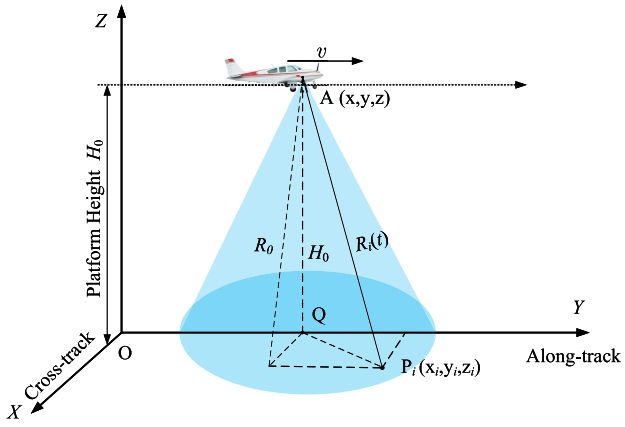

Fig. 1. SARAL geometry.

system $O-XYZ$ is established with O as the origin. Assuming that the antenna phase center (APC) of the radar altimeter is located in $A(x,y,z)$ at time t. The illumination scene is shown on the ground in Fig. 1. Q is the scene center, P_i is a scatter located in illuminated scene, whose coordinate is (x_i,y_i,z_i). Therefore, the slant distance from APC to the scatter is R_i as

$$\begin{aligned} R_i &= \sqrt{(x-x_i)^2+(y-y_i)^2+(z-z_i)^2} \\ &= \sqrt{x_i^2+(v\eta-y_i)^2+H_0^2}. \end{aligned} \tag{1}$$

It is not difficult to see that when $x=0$, there is $z=H_0$, $z_i=0$, $y=v\eta$, and η denotes slow time variable. Setting that $R_0=\sqrt{H_0^2+x_i^2}$ is the minimum reference slant distance where the direction of R_i is perpendicular to along-track. Generally, if $|v(\eta-\eta_0)| \ll R_0$, then the range equation shaped like a hyperbola R_i and it can be approximated as a parabola

$$\begin{aligned} R_i &= \sqrt{R_0^2+v^2(\eta-\eta_0)^2} \\ &\approx R_0+\frac{v^2}{2R_0}(\eta-\eta_0). \end{aligned} \tag{2}$$

To obtain the height information of the scatter, the LFM signal is transmitted, which can be expressed as

$$s_t(t)=A_0\text{rect}\left(\frac{t}{T_p}\right)\exp\left(j2\pi(f_ct-\frac{1}{2}K_rt^2)\right) \tag{3}$$

where $K_r=B/T_p$ is the chirp rate of transmitting frequency, B is the frequency bandwidth, and T_p is the pulsewidth, respectively. In (3), f_c is the carrier frequency and t is the time variable (or cross track time). A_0 is the amplitude of the transmitted signal. Airborne platforms usually cannot accurately fly along a predetermined track, and will result in motion deviations, which can be denoted as Δr. After a certain delay, the received echo can be obtained as the form of

$$\begin{aligned} s_r(t,\eta) &= A_0\sigma^0\text{rect}\left(\frac{t-\tau}{T_p}\right)\exp\left[j2\pi f_c(t-\tau)\right] \\ &\quad\times\exp\left[-j\pi K_r(t-\tau)^2\right]\exp\left(j\Delta\phi\right)+n\left(t,\eta\right) \end{aligned} \tag{4}$$

where $\tau = \tau(\eta) = 2R(t,\eta)/c$ is two-way delay of radar to target scatter under the stop-and-go approximation [15] and $\Delta\phi = 4\pi\Delta r/c$ is the NsPE caused by the platform motion error, which is the multiplicative error reflected on the echoes. In (4), σ^0 is the scattering coefficient, $n(t,\eta)$ is additive noise or clutter, and η is slow-time, which is related to the along-track movement of SARAL. It is worth noticing that τ has no analytical form, which will be estimated in the following discussion. For the convenience of expression, $A_0\sigma^0$ is omitted in the following derivation.

III. Long Coherent Processing

With the signal processing of SAR imagery for reference, the coherent processing interval is synthetic aperture time instead of conventional burst interval. All the echoes in the illuminating time will be collected and coherently accumulated, which can improve the along-track resolution. The long coherent processing mainly includes two stages. In the first stage, the dechirp (or deramp) in cross-track, range cell migration correction (RCMC), range compression residual video phase (RVP) correction, and NsPE estimation are completed in a subaperture manner. In the second stage, the NsPE phase is spliced into full-aperture phase errors and iteratively corrected. Finally, along-track long coherent accumulation, i.e., along-track fast Fourier transform (FFT), is designed to obtain a fully focused 2D-DDM.

A. Systematic Phase Error Compensation

Usually, the received echo needs a dechirp (deramp) processing, which is similar to matched filtering process [16]. After multiplying the received echo with the delayed replica of the transmitted signal, the beat signal can be obtained as follows:

$$\begin{aligned} s_{if}(t,\eta) &= s_r(t,\eta) \times {s_{ref}}^*(t,\eta) \\ &= \text{rect}\left(\frac{t-\tau}{T_p}\right)\exp\left(j2\pi\left(f_c\tau' - K_r\tau' t + \frac{1}{2}K_r{\tau'}^2\right)\right) \\ &\quad \times \exp\left(j\Delta\phi\right) + n\left(t,\eta\right) \end{aligned} \tag{5}$$

where

$$\begin{aligned} s_{\text{ref}}(t) &= s_t(t-\tau_{\text{ref}}) \\ \tau' = \tau - \tau_{\text{ref}} &= \frac{2(R_i - R_{\text{ref}})}{c} \end{aligned} \tag{6}$$

where R_{ref} is tracker reference slant, which is obtained by airborne tracker [1]. What is worth noting is that (5) is a continuous wave signal for time t with a frequency of $K_r\tau'$.

Note that according to (2), τ' can be further written as

$$\tau' = \frac{2(R_0 - R_{\text{ref}})}{c} + \frac{v^2}{cR_0}(\eta-\eta_0)^2 = u + \frac{v^2}{cR_0}(\eta-\eta_0)^2 \tag{7}$$

where $\frac{v^2}{R_0}(\eta-\eta_0)^2$ is the range migration term, u is the difference between the minimum two-way travel delay, and the tracker reference slant delay. The RCMC process is completed by multiplying the corresponding compensated phase, as is shown below

$$\begin{aligned} s_{RCMC}(t,\eta) &= s_{if}\cdot\exp\left(j2\pi\frac{v^2}{R_0}(\eta-\eta_0)^2 t\right) \\ &= \text{rect}\left(\frac{t-\tau}{T_p}\right)\exp\left(j2\pi\left(f_c\tau' - K_r u t + \frac{K_r}{2}{\tau'}^2\right)\right) \\ &\quad \times \exp(j\Delta\phi) + n(t,\eta) \end{aligned} \tag{8}$$

where the first term is a Doppler term, which is related to the along-track Doppler frequency. The second term is continual wave (CW), which is exactly what we need, and the third item is RVP, which needs to be removed. After RCMC, to focus in the cross-track, range compression is required, which can be achieved by delay IFFT as follows:

$$\begin{aligned} s_{RC}(f_r,\eta) &= \mathcal{F}[s_{i,RCMC}] = \int_{T_i}^{T_i+T_p} s_{i,RCMC} \\ &\quad \exp(-j2\pi f_r t)dt \\ &= T_p\text{sinc}\ \left[T_p\left(f_r{\tau_i}' - \gamma u_i\right)\right]\exp\left[j2\pi\left(f_c{\tau_i}' + \frac{\gamma}{2}{{\tau_i}'}^2\right)\right] \\ &\quad \times \exp\left(j\Delta\phi\right) + n\left(f_r,\eta\right). \end{aligned} \tag{9}$$

Considering that the frequency f_r can be expressed by $f_r = K_r\tau_r$, which is directly related to the time delay, $s_{i,RC}(\tau_r,\eta)$ can be further approximated as

$$\begin{aligned} s_{RC}(\tau_r,\eta) &= T_p\text{sinc}\left[B(\tau_r - u)\right]\exp\left(j2\pi\left(f_c\tau' + \frac{K_r}{2}{\tau'}^2\right)\right) \\ &\quad \times \exp\left(j\Delta\phi\right) + n\left(\tau_r,\eta\right) \end{aligned} \tag{10}$$

where B is the signal bandwidth, τ_r denotes the time delay in the altimeter measure window. It is worth noting that, after RCMC and range compression, the response of a single scatterer is concentrated at the time delay $\tau_r = u$ in the window, which means that the slant distance between the scatterer and the altimeter is the minimum.

After range compression, RVP correction is required. From (10), the signal after RVP correction can be written as

$$\begin{aligned} s_{RVP}(\tau_r,\eta) &= s_{RC}\cdot\exp\left(j2\pi\left(\frac{K_r}{2}{\tau'}^2(\eta)\right)\right) \\ &= T_p\text{sinc}\left[B(\tau_r - u)\right]\exp\left(j2\pi(f_c\tau')\right) \\ &\quad \times \exp\left(j\Delta\phi\right) + n(\tau_r,\eta) \end{aligned} \tag{11}$$

where both RVP and range migration are systematic phase errors (SPE). However, $\exp(j\Delta\phi)$ are non-systematic phase errors. There is no analytical form to calculate. The NsPE can be compensated only by the data-driven phase error autofocusing algorithm. The phase gradient autofocusing (PGA) algorithm is proved to be a classic autofocusing algorithm, which is widely used in the SAR imagery.

B. Nonsystematic Phase Error Compensation

The phase error is obtained by PGA algorithm through the phase gradient estimating of echoes, and then the phase error is integrated from phase error gradient. Then, phase compensation

can be realized. The PGA algorithm mainly includes four steps: center (circular) shifting, windowing, phase gradient estimation, and iterative correction. In the first step, the strongest scatters are selected and moved to the center of the image (the center of the image), whose purpose is to eliminate the Doppler frequency shift of the scatters. The second step is to window the cyclically moving image so that each range bin contains as much scattered energy as possible, while discarding the data that do not contribute to the phase error, which allows the highest signal-to-noise ratio (SNR) data to be used for phase error estimation. The third step is to estimate the phase error gradient by the linear unbiased minimum variance (LUMV) estimation, and the phase error function $\Delta\hat{\phi}$ can be obtained through the integral operation. The echo data are multiplied by the complex conjugate of the phase error function and the correction process is finished. However, the estimation and correction steps must be repeated iteratively to continuously eliminate phase errors. As the image becomes more and more focused, the single scatterer becomes more compact, the SNR is improved, and the algorithm tends to converge. The echoes after NsPE $\Delta\phi$ are corrected as follows:

$$\begin{aligned} s_{\mathrm{PGA}}(\tau_r,\eta) &= s_{RVP}\cdot\exp\left(j\Delta\hat{\phi}\right) \\ &\approx T_p\mathrm{sinc}\left[B(\tau_r-u)\right]\exp\left(j2\pi(f_c\tau')\right)+n(\tau_r,\eta) \end{aligned} \tag{12}$$

C. 2D-PTR of Echoes

Long correlation processing is realized by coherently combining the echoes along the along-track within its illuminating time. Considering the long correlation processing of the along-track position y_p

$$\begin{aligned} s(\tau_r,\eta) &= \sum_{\eta} s_{PGA}(\tau_r,\eta)\exp[-j2\pi f_c\tau'_{y_p}(\eta)] \\ &= T_p\mathrm{sinc}\left[B(\tau_r-u)\right] \\ &\quad\times\sum_{\eta}\exp\left(j2\pi f_c(\tau'(\eta)-\tau'_{y_p}(\eta))\right)+n(\tau_r,\eta) \end{aligned} \tag{13}$$

where $\tau'(\eta)-\tau_{y_p}{}'(\eta)\approx(2y_py-y_p^2)/cR_0$, and $y=v\eta$ denotes the position in along-track. Substituting $\tau_i{}'(\eta)-\tau_{y_p}{}'(\eta)$ into (13), the signal function can be rewritten as

$$\begin{aligned} s(\tau_r,\eta) &= T_p\mathrm{rect}\left(\frac{t}{T_p}\right)\mathrm{sinc}\left[B(\tau_r-u)\right] \\ &\quad\times\sum_{\eta}\exp\left(j2\pi\frac{y_pv\eta+y_p^2}{\lambda R_0}\right)+n(\tau_r,\eta) \end{aligned} \tag{14}$$

where $\sum_\eta\exp(\cdot)\approx\int_{-T_i/2}^{T_i/2}\exp(\cdot)d\eta$, and T_i is the coherent processing time along-track, which is CPI or synthetic aperture time T_{SAR}, and it is not the burst duration. Usually, the Doppler frequency can be denoted as

$$f_d=\frac{2v\sin\theta}{\lambda}\approx\frac{2y_pv}{\lambda R_0}. \tag{15}$$

Replacing the relevant variable with Doppler frequency f_d, the echo $s(\tau_r,\eta)$ can be further expressed as

$$\begin{aligned} s(\tau_r,\eta) &\approx T_p\mathrm{rect}\left(\frac{t}{T_p}\right)\mathrm{sinc}\left[B(\tau_r-u)\right]\exp\left(j2\pi\frac{y_p^2}{\lambda R_0}\right) \\ &\quad\times\int_{-T_i/2}^{T_i/2}\exp(j\pi f_d\eta)d\eta+n(\tau_r,\eta). \end{aligned} \tag{16}$$

After further calculation, the echo can be written as

$$\begin{aligned} s(\tau_r,f_d) &= T_pT_i\mathrm{rect}\left(\frac{t}{T_p}\right)\mathrm{sinc}\left[B(\tau_r-u)\right]\mathrm{sinc}\left[T_if_d\right] \\ &\quad\times\exp\left(j2\pi\frac{y_p^2}{\lambda R_0}\right)+n(\tau_r,f_d) \\ &\approx T_pT_i\mathrm{rect}\left(\frac{t}{T_p}\right)\mathrm{sinc}\left[B(\tau_r-u)\right]\mathrm{sinc}\left[T_if_d\right] \\ &\quad+n(\tau_r,f_d) \end{aligned} \tag{17}$$

where the echo is in the range-delay and azimuthal-Doppler domain. The 2-D echo has high main lobe energy at $y_p=0$, $\exp(j2\pi y_p^2/\lambda R_0)\approx 1$. To this end, the altimeter echo is finally expressed as a 2D sinc function related to the delay τ_r and Doppler frequency f_d, which is also the origin of the name delay/Doppler altimeter. Equation (17) is also called 2-D point target response (2D-PTR) of SARAL.

D. Long Coherent Processing Procedures

The previous section derives the long coherent processing theoretically and mathematically. The procedures mainly include range dechirp, RCMC, range compression, RVP correction, NsPE correction, and along-track FFT. To understand the processing procedures, the long coherent processing is divided into seven stages, as shown in Fig. 2, which are as follows:

Stage 1. Subaperture segmentation: In order to achieve high-precision processing of the long synthetic aperture echo data, subaperture processing is an effective method. Therefore, the full-aperture echoes are segmented into several overlapped subaperture data blocks. This overlapped subaperture data are to avoid phase discontinuities when connecting. The following stages 2 to 5 are all completed in a subaperture manner.

Stage 2. Range deramp: Range deramp is a widely used technology for current radar altimeters, which is also known as deramp-on-receive technique. It achieved echo matched filtering based on an analog mixer. After the processing, the output signal becomes an intermediate frequency signal or beat signal. Usually, this process is completed by multiplying the received echo by a complex conjugate of the transmitted signal with a certain delay, in which the delay is obtained by the on-board range gate tracker.

Stage 3. RCMC and range IFFT: Since the range is constantly changing from altimeter to the target scatter, the echo from the same scatter will be distributed in several adjacent range gates, the delay compensation is needed, which is similar to SAR imaging RCMC, we call it range cell migration correction in this article. As shown in (8) in the previous section, by

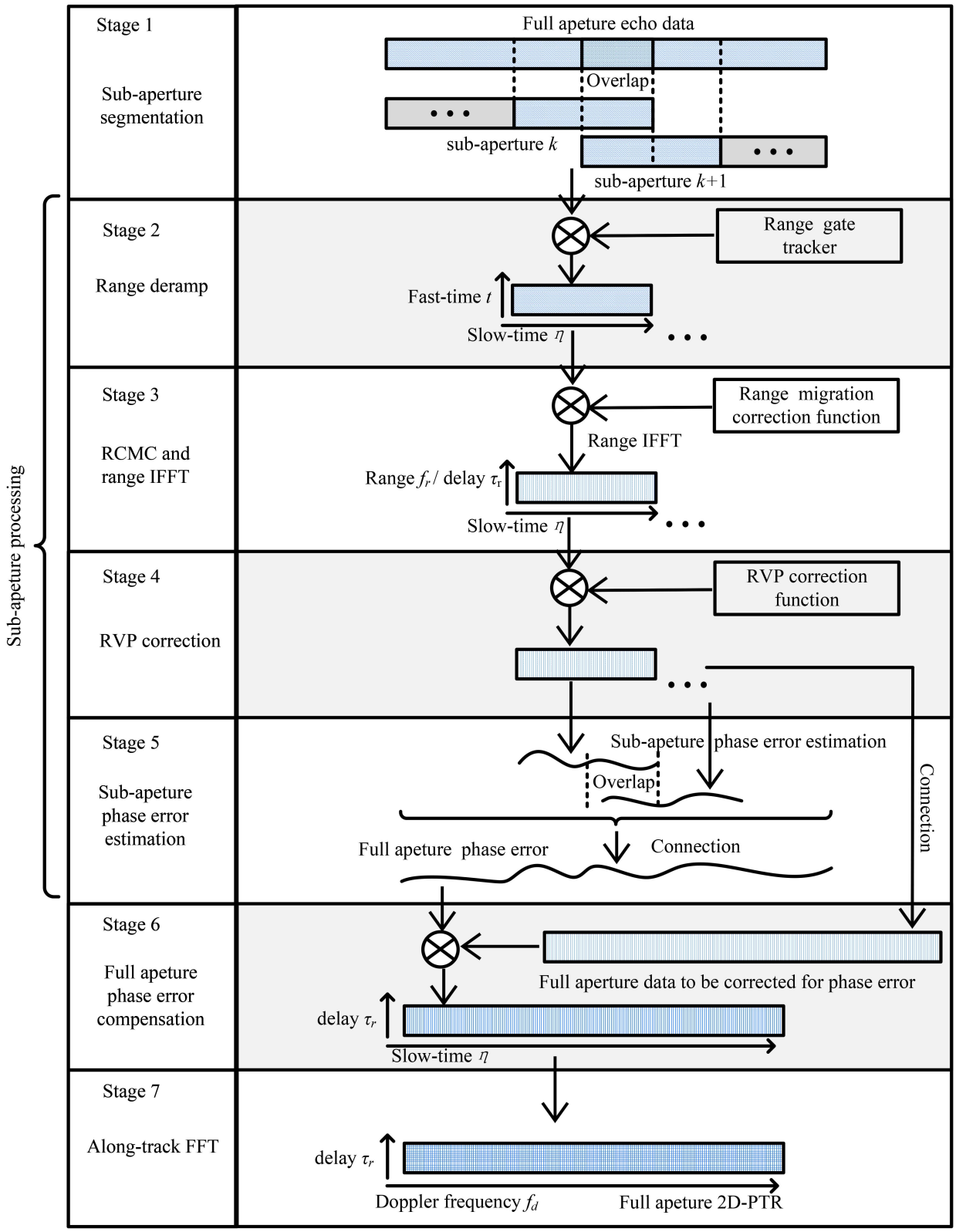

Fig. 2. Flowchart of long coherent processing.

constructing a range migration multiplier, the range migrations can be corrected. After RCMC, range IFFT guarantees the echo cross-track focused. To this end, the echo is slow-time domain in along-track, and range frequency domain in cross-track. Due to $f_r = K_r \tau_r$, the echo can also be regarded as a function of delay τ_r in cross-track.

Stage 4. RVP correction: The RVP correction as shown in (11). It is worth mentioning that RVP is the second order phase of the delay, which will also produce Doppler frequency, but the influence on the phase is much smaller than the Doppler term. However, its impact cannot be ignored. RVP can be corrected by multiplying the corresponding matched filter function.

Stage 5. Subaperture phase error estimation: After RCMC and RVP correction, the systematic phase error is basically corrected. Due to various factors such as turbulence, the altimeter platform cannot accurately fly along to the planned route, causing NsPE, which is random and will produce targets image defocus. Therefore, the NsPEs are different from range migration error and RVP, which have no analytical form and can only be estimated by specific algorithms. PGA is a classic algorithm. After estimating the phase gradient, the phase error function is obtained through the integral calculation.

Stage 6. Full-aperture phase error compensation: The subaperture echo data after the RVP correction is connected to a full-aperture echo data, which is the echo after systematic phase errors correction. Multiplying the full-aperture data by the conjugate of the full-aperture phase error function estimated by the PGA algorithm, the NsPE can be corrected.

Stage 7. Along-track FFT: After the phase error is corrected, this stage is mainly to realize the focusing of the along-track. This process can be completed by the FFT (slow-time coherent summation) along-track. As shown in Fig. 2, the echo after the along-track FFT is at delay Doppler domain, which is 2D-PTR.

IV. Altimetry Parameter Retracking

In this section, the altimeter parameter retracking will be discussed. In 2D-PTR, the Doppler beams are related to different along-track positions, and the range gate (delay) is involved in the height information. Brown [17] showed that the echo of SARAL follows the analytical model formed by the convolution of flat surface response and topographic distribution. It considers factors such as antenna pattern, illumination scene geometry, and surface backscattering coefficient. Based on this analytical model, the height parameter estimation algorithms of the least squares algorithm (LS) and the maximum likelihood (MLE) method can be utilized, which are the most commonly used estimation algorithms. However, although the LS and MLE algorithms are simple and efficient, they are susceptible to noise. Therefore, a flexible Bayesian learning framework is designed in this section, where the prior is set by a GGD. To accommodate for the statistically complicated prior, the Bayesian learning is performed in a hierarchical manner, and HMC sampler is introduced to obtain closed-form solutions of the height parameter posterior.

To access the height parameter, a proper parameter model is necessary. According to the existing literature, a convolution model is as follows [18]:

$$g(t, f_n) = p_{FSR}(\tau_r, f_n) * w(t) \tag{18}$$

where $w(t)$ is the topographic distribution, which is a probability density function. $p_{FSR}(\tau_r, f_n)$ is the flat surface response of a single Doppler beam, where n represents the different along-track positions or perspectives. In addition, $t = t_0 + \tau_r$, where t_0 is the retracking observation window delay of the received echo. Then, $w(t)$ can be expressed as the function $w(\tau_r)$, $w(\tau_r)$, and $p_{FS}(\tau_r, f_n)$ can be further denoted as

$$w(\tau_r) = \frac{1}{\sqrt{2\pi}\sigma_s} \exp\left(-\frac{(t_0 + \tau_r)^2}{2\sigma_s^2}\right) \tag{19}$$

$$p_{FSR}(\tau_r, f_n) = \frac{\lambda^2}{(4\pi)^3} \int_A \frac{G^2(\rho,\theta)\sigma^0(\rho,\theta)s(\tau_r, f_n)}{R^4(\rho,\theta)} \rho d\rho d\theta \tag{20}$$

where $\sigma_s = SWH/2c$, and SWH is the effective wave height parameter. σ^0 is the normalized radar cross section (RCS), G is the antenna gain, and f_n denotes the Doppler frequency of the nth along-track beam. In addition, R is the distance of altimeter to the scatterers, which is determined by ρ and θ. A is the area of the illuminated scene, and (ρ, θ) is the coordinate of any points in the scene expressed with polar coordinate format. $s(\tau_r, f_n)$ is a 2-D PTR, which can be approximated as

$$s(\tau_r, f_n) = \text{sinc}\left[B\left(\tau_r - 2R(\rho,\theta)/c\right)\right] \text{sinc}\left[T_i\left(f_d(\rho,\theta) - f_n\right)\right]. \tag{21}$$

Since σ^0 and R change slowly with the illumination scene, it can be assumed as a constant value and denoted by P_u, which is called the echo amplitude, i.e., $P_u = \lambda^2\sigma^0/4\pi^3R^4$. Then, p_{FSR} can be further expressed as

$$p_{FSR}(\tau_r, f_n) = P_u \int_A G^2(\rho,\theta) s(\tau_r, f_n) \rho d\rho d\theta. \tag{22}$$

To simplify the integration calculation of (22), the antenna pattern and 2-D sinc function of 2D-PTR can be approximated by Gaussian function [13]. The altimeter echo $g(t, f_n)$ is still in 2-D form. In order to obtain the 1-D echo of the altimeter, multilooking processing is necessary.

The multilooking processing is achieved by incoherently summation of the echo on different Doppler beams at different along-track positions, which is to obtain a better along-track resolution. The final 1-D altimeter echo is as

$$g(\tau_r) = \sum_{n=1}^{N} g(\tau_r, f_n) \tag{23}$$

where $g(\tau_r)$ is an M-dimensional vector, which is actually a function of three height parameters: echo delay τ_r, effective wave height SWH, and echo amplitude P_u. For the sake of simplicity, we only express it as a function of τ_r. Therefore, the echo mathematical model (23) can be used to retrack [5] and estimate the height parameters.

In the altimeter signal processing flow, the height parameter estimation is the last link. Since the estimation of radar altimeter parameters must be carried out within the observation window,

this stage is usually called ground retracking. The existing LS and MLE algorithms only consider the independence of the altimeter echo and estimate a series of parameters at a time [19]. The statistical properties of the echo parameters and the prior characteristics of the echo are not considered. Hence, a statistical estimation algorithm based on HMC sampling technology is proposed in this article. This algorithm establishes a Bayesian inference model by considering the statistical properties of the echo parameters to realize altimetry parameter estimation. For the convenience of presentation, the 1-D echo $g(\tau_r)$ of the altimeter is thickened to emphasize that it is an M-dimensional vector. The specific estimation model can be expressed as

$$\mathbf{y} = \mathbf{g}(\tau_r) + \mathbf{e} \tag{24}$$

where $y \in \mathbb{R}^M$ is the observed echo, $\mathbf{g}(\tau_r) \in \mathbb{R}^M$ is the unknown noiseless echo, and $\mathbf{e} \in \mathbb{R}^N$ is the additive noise. Note that echo delay parameter τ_r is related to the echo, which can be estimated according to (23). In Bayesian estimation, prior models, likelihood, and Bayesian inference will be discussed.

A. Flexible Prior and Likelihood Model

First, to carry out the first Bayes for DDM feature enhancement, the echo delay τ_r is modeled as the GGD prior. GGD is flexible to characterize the altimetry echo prior information, thereby high-precision parameter estimation can be obtained. In such a case, the prior is denoted as

$$\begin{aligned} p(\tau_r|\alpha,\beta) &= \mathcal{GGD}(\tau_r|\alpha,\beta) \\ &= \frac{1}{2\alpha^{1/\beta}\Gamma(1+1/\beta)} \exp\left(-\frac{|\tau_r|^\beta}{\alpha}\right) \end{aligned} \tag{25}$$

where $\Gamma(\cdot)$ is the gamma function and $\alpha > 0, 0 \le \beta \le 2$ are the scale parameter and shape parameters of GGD, respectively. The GGD distribution represents different distributions with different shape parameters. When $\beta = 1$, GGD is Laplace distribution. If $\beta = 2$, GGD is Gaussian distribution. $\beta \to 0$, the sparser the prior, and $\beta \to 2$, the smoother the prior. Therefore, the GGD is a flexible prior distribution, which can represent different degrees of sparsity.

Equation (25) describes the statistical characteristics of the parameter τ_r, and therefore, it becomes a random variable to be estimated. According to the Bayesian estimation framework, the likelihood function is usually determined by the noise model of the signal. Considering that additive noise is usually Gaussian white noise, the likelihood function can be expressed as

$$p(\mathbf{y}|\tau_r,\sigma^2) = \left(\frac{1}{\sqrt{2\pi}\sigma}\right)^M \exp\left(-\frac{\|\mathbf{y}-\mathbf{g}(\tau_r)\|_2^2}{2\sigma^2}\right) \tag{26}$$

where σ^2 is the noise variance and $\|\cdot\|_2$ denotes the ℓ_2 norm of vector. Note that the observed echo $\mathbf{y}$ is also Gaussian, and the variance is σ^2. Since the prior GGD is not conjugate to Gaussian likelihood, which results in nonclosed solution. To this end, the hierarchical Bayesian model is introduced, which designs a certain probability distribution for each parameter to construct the relationship between prior and likelihood.

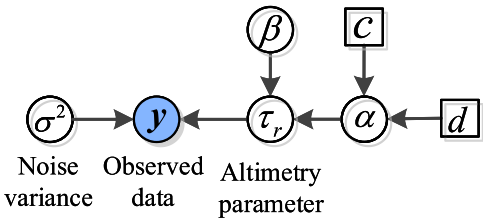

Fig. 3. DAG of Bayesian modeling for altimetry parameter retracking.

B. Bayesian Hierarchical Model

The parameter σ^2 is the noise variance, in order to ensure that it is always positive, and provide no information as much as possible, it can be designed as Jeffrey's noninformation prior

$$p(\sigma^2) \propto \frac{1}{\sigma^2}\mathcal{I}_{\mathbb{R}^+}(\sigma^2) \tag{27}$$

where $\mathcal{I}_{\mathbb{R}+}$ is the indicator function on $\mathbb{R}+$. Note that when $\sigma^2 \in \mathbb{R}+$, $\mathcal{I}_{\mathbb{R}^+}(\sigma^2) = 1$, and 0 otherwise. For more information on this a prior hypothesis, please refer to [20]. The scale parameter of GGD is positive number and needs to be conjugate to the Gaussian distribution, which can be defined as the inverse gamma distribution

$$p(\alpha|c,d) = \mathcal{IG}(\alpha|c,d) = \frac{d^c}{\Gamma(c)}\alpha^{-c-1}\exp\left(-\frac{d}{\alpha}\right)\mathcal{I}_{\mathbb{R}+}(\alpha) \tag{28}$$

where c and d are fixed constant parameters, and its experience value is usually 10^{-3}, and $\mathcal{IG}(\cdot)$ represents the inverse gamma distribution. Next, the shape parameter β belongs to the interval $[0, 2]$. It can be assumed to be a uniform distribution, that is, $\beta \sim \mathcal{U}_{[0,2]}$, which can ensure the high flexibility and sparsity of GGD prior. After the Bayesian hierarchical model is constructed, the relationship of these variables and hyper-parameters can be expressed in the form of a directed acyclic graph (DAG), as shown in Fig. 3.

Fig. 3 shows the relationship of various parameters in the retracking technique of altimetry parameters under Bayesian hierarchical model. The displayed random variable $\mathbf{y}$ represents the observation data, which is the 1-D altimeter echo signal obtained after correction. τ_r indicates the altimetry parameter to be restored. α, β, and σ^2 are all latent random variables, which represent the scale parameters, shape parameters, and noise variance of GGD, respectively.

In Bayesian inference, the molecule is the product of prior function and likelihood function, which is required to be conjugate. Otherwise the closed solution of the posterior probability density function can not be obtained under the Bayesian framework. The conjugate relationship between likelihood distribution function and prior distribution function can be constructed by introducing hyper parameters. Therefore, the hierarchical Bayesian model is constructed. According to (25) and the likelihood function (26), the joint posterior distribution can be

expressed as

$$p(\tau_r,\alpha,\beta,\sigma^2|\mathbf{y})=\frac{p(\tau_r|\alpha,\beta)p(\alpha|c,d)p(\beta)p(\mathbf{y}|\tau_r,\sigma^2)p(\sigma^2)}{p(\mathbf{y})} \tag{29}$$

where $p(\mathbf{y})$ can be regarded as a normalization constant, and the joint distribution is proportional to the product of the prior and the likelihood function of each parameter. Since the full Bayesian estimation is desired, which means that the exact values of all parameters can be estimated. Therefore, the conditional posterior of the altimetry parameter τ_r and the hyper-parameter α, β, σ^2 can be obtained by marginal calculation. The conditional posterior of scale parameter of GGD can be expressed as

$$p\left(\alpha|\tau_r,\mathbf{y},\beta,\sigma^2\right)\propto\mathcal{IG}\left(\alpha|c+1,d+|\tau_r|^\beta\right). \tag{30}$$

Note that (30) is still the inverse gamma distribution, which is a typical distribution function and can be sampled by the classic Gibbs algorithm [21]. Then, the posterior of shape parameter β can be obtained by (25) and uniform distribution $\beta\sim\mathcal{U}_{[0,2]}$, which have the form of

$$p\left(\beta|\tau_r,\mathbf{y},\alpha,\sigma^2\right)\propto\frac{1}{2\alpha^{1/\beta}\Gamma(1+1/\beta)}\exp\left(-\frac{|\tau_r|^\beta}{\alpha}\right)\mathcal{I}_{[0,2]}(\beta) \tag{31}$$

where (31) is GGD defined as [0,2], which is an atypical distribution function cannot be sampled by the Gibbs algorithm mentioned above. To this end, the Metropolis Hastings (MH) is a popular solution, which is capable of sampling the atypical distribution effectively.

Similarly, according to (26) and (27), the conditional posterior of noise variance σ^2 can be calculated as

$$p(\sigma^2|\tau_r,\mathbf{y},\alpha,\beta)\propto\mathcal{IG}\left(\sigma^2|\frac{M}{2},\frac{\|\mathbf{y}-\mathbf{g}(\tau_r)\|_2^2}{2}\right) \tag{32}$$

where (32) is also an inverse gamma distribution, similar to (30), and thus Gibbs can be used as the suitable sampling method.

In addition, the posterior of the altimetry parameter τ_r can be calculated by (25) and (26). Since the altimeter echo delay τ_r and shape parameter β are usually positive, i.e., $|\tau_r|^\beta=(\tau_r)^\beta$, the marginal posterior distribution of echo delay parameters τ_r is expressed as

$$p(\tau_r|\mathbf{y},\alpha,\beta,\sigma^2)\propto\exp\left[-\frac{(\tau_r)^\beta}{\alpha}-\frac{\|\mathbf{y}-\mathbf{g}(\tau_r)\|_2^2}{2\sigma^2}\right]. \tag{33}$$

Note that the posterior in (33) is a typical distribution, and the sampling processing cannot be implemented with the classic Gibbs algorithms, while the MH is not so efficient due to the random walk strategy. To this end, an effective statistical sampling algorithm is proposed, which is based on the Hamiltonian dynamic model. The HMC can cope with the problem of estimating from the complicated and atypical PDF. Its estimate process is to generate a large number of samples through Monte Carlo random simulation according to the related PDF, and then the expectation of these samples is calculated and considered as the estimated values. In the HMC framework, according to the conservation principle of kinetic energy and potential energy, the total energy function is constructed as

$$H(\tau_r,\mathbf{q})=U(\tau_r)+K(\mathbf{q}) \tag{34}$$

where $U(\cdot)=(\tau_r)^\beta/\alpha+\|\mathbf{y}-\mathbf{g}(\tau_r)\|_2^2/2\sigma^2$ is the potential function of the posterior of echo delay parameters, $K(\mathbf{q})=\mathbf{q}^{\mathrm{T}}\mathbf{q}/2$ is the kinetic energy function, and $\mathbf{q}\in\mathbb{R}^M$ is the momentum of the object. Note that $\mathbf{q}$ is a M dimensional vector and τ_r is a scalar, while $U(\tau_r)$ and $K(\mathbf{q})=\mathbf{q}^{\mathrm{T}}\mathbf{q}/2$ are scalar functions. The HMC algorithm performs variable update sampling according to the leapfrog step, the iteration process of HMC estimation is

$$\mathbf{q}^{(t,(i+1/2)\delta)}=\mathbf{q}^{(t,i\delta)}+\frac{\delta}{2}\nabla U\left({\tau_r}^{(t,i\delta)}\right) \tag{35}$$

$${\tau_r}^{(t,(i+1)\delta)}={\tau_r}^{(t,i\delta)}+\delta\mathbf{q}^{(t,(i+1/2)\delta)} \tag{36}$$

$$\mathbf{q}^{(t,(i+1)\delta)}=\mathbf{q}^{(t,(i+1/2)\delta)}+\frac{\delta}{2}\nabla U\left({\tau_r}^{(t,i\delta)}\right) \tag{37}$$

where i is the number of leapfrog, δ is the leapfrog step length, r is the number of iterations, and $\nabla(\cdot)$ is the gradient operator, which is denoted as

$$\nabla(\tau_r)=\frac{\beta(\tau_r)^{\beta-1}}{\alpha}-\left(\mathbf{y}^{\mathrm{T}}-\mathbf{g}^{\mathrm{T}}(\tau_r)\right)\cdot\frac{d\mathbf{g}(\tau_r)}{d\tau_r}. \tag{38}$$

It is worth noting that the momentum variable $\mathbf{q}$ is updated with half a leap as the step length, and the update step length of echo delay parameter τ_r is a total leapfrog, and they iterate alternately. After I times iterations, the algorithm converges, and the candidate sample ${\tau_r}^*={\tau_r}^{(t,I\delta)}$ and $\mathbf{q}^*=\mathbf{q}^{(t,I\delta)}$ are obtained. The candidate samples should be further judged using the "receive-reject" step of the MH algorithm to determine whether they follow the target distribution. After t correct samples $\{{\tau_r}^1,{\tau_r}^2,\cdots{\tau_r}^t\}$ and $\{\mathbf{q}^1,\mathbf{q}^2,\cdots\mathbf{q}^t\}$ are obtained, judge the current candidate ${\tau_r}^*$ and $\mathbf{q}^*$ whether it can be served as the $(t+1)$th sample. The probability of reception is expressed as

$$\min\left\{1,\exp\left(H({\tau_r}^t,\mathbf{q}^t)-H({\tau_r}^*,\mathbf{q}^*)\right)\right\}. \tag{39}$$

If the candidate sample is received, ${\tau_r}^{t+1}={\tau_t}^*$, $\mathbf{q}^{t+1}=\mathbf{q}^*$, otherwise ${\tau_r}^{t+1}={\tau_r}^t$, $\mathbf{q}^{t+1}=\mathbf{q}^t$.

The sampling estimation methods of scale parameter α, shape parameter β, noise variance σ^2, and altimeter delay parameter τ_r are discussed above. When the maximum number of iterations $T_{\max}$ is reached, the estimation process ends and the estimation of full Bayesian can be obtained.

V. Processing Procedure

In this section, we are to discuss the processing procedure of the proposed algorithm as shown in Fig. 4. In Section III-D above, a 2-D DDM is obtained. To this end, the DDM will serve as the input of the Bayesian retracking process. First, a multilooking process is exploited to obtain a 1-D altimeter echo according to the altimetry principle, which aims at gathering all the reflected energies from a single Doppler beam. After RCMC, RVP, and NsPE correction, the starting time of echo of the same

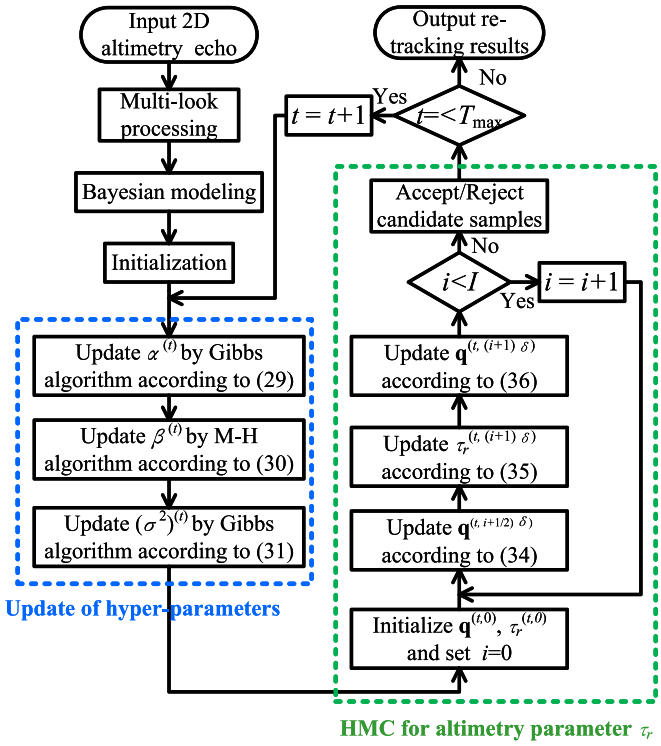

Fig. 4. Processing procedure of the proposed algorithm.

target height in the same synthetic aperture are the same. It allows us to sum to obtain the multilooking waveform as (23).

Then, based on the existing convolution model, the altimeter echo parameters are modeled as random variables, which follow flexible GGDs. The Bayesian inference framework is utilized to obtain the posterior distribution of the altimetry parameters and the introduced hyper-parameters, which is expected to achieve full Bayesian estimation. For the scale parameter α, shape parameter β of GGD prior, and noise variance σ^2, the suitable sampling algorithm are introduced to implement the iterative update of the sampling process. Due to the posterior of the altimeter parameter τ_r is complex and atypical, the traditional sampling algorithms, such as Gibbs and MH cannot solve it, hence the newly HMC is exploited to realize its sampling estimation. In HMC, the momentum variable $\mathbf{q}$ and the altimeter parameter τ_r are updated alternately through leapfrog steps, the iteration is stopped after reaching a certain number of convergence times, and the "accept–reject" criterion is used to judge whether the candidate sample is a suitable sampling value. Finally, the altimeter parameter achieves retracking, and the ground altitude can be calculated by the obtained gate number τ_r.

VI. Experiments

In this section, the effectiveness and superiority of the proposed algorithm are verified through SARAL raw data experiments. The experimental results obtained at each processing stage will be displayed and quantitatively analyzed in this section. The raw data acquisition parameters are listed in Table I. Under the set of parameters, a set of original echoes are obtained

TABLE I
System Parameters of the Airborne Altimeter

Platform velocity (v)	66 m/s
Carrier frequency (F_c)	2.8 GHz
Bandwidth (B)	100 MHz
Pulse repetition frequency (PRF)	2000 Hz
Sampling frequency (F_s)	125 MHz
Pulse width (T_p)	5 μs
Nearest slant range (R_0)	2300 m

as shown in Fig. 5, the echo's along-track and cross-track size are $40\,000 \times 1024$. To perform subaperture processing, the echoes are divided into 72 blocks and loaded then processed in the form of overlapped subapertures. The size of each block is 1024×1024, and the overlapped part is 1/2 of the along-track of each block. Therefore, the along-track length is 37 376. From Fig. 5, the along-track and cross-track are corresponding to the route direction of the altimeter flight and the direction perpendicular to the route, respectively. The vertical line in the Fig. 5 may be the direct power component of the echo, which will be eliminated in the later processing.

The raw data are processed through a long coherent processing step as shown in Fig. 2. Since the airborne altimeter platform is always moving, the relative distance between the altimeter and the target scattering point on the ground surface is constantly changing. Therefore, the delay error is produced in along-track, which is similar to the range migration in SAR imagery, we also call it range migration in this article. Fig. 6(a) shows the echoes of long coherent processing result after RCMC and range compress, while the results of five subapertures before RCMC and after RCMC are shown in Fig. 6(b), (c). From Fig. 6(a), we can observe that ups and downs of terrain in long along-track. Fig. 6(b), (c) initially shows the RCMC performance of the five subapertures. Since the area corresponding to the five subapertures is relatively flat, the altitudes are roughly the same.

In order to observe the change of echo before and after RCMC more clearly, one of the subaperture results is selected for comparison and analysis, as shown in Fig. 7(a) and (b). It can be seen from Fig. 7 that, before RCMC processing, the delay error of the echo is relatively large and the echo power is curved in a hyperbolic manner. For the convenience of processing, we approximate the range migration to a parabola, and the analytical form is as shown in (2). The approximation is widely used in SAR signal processing [15]. The echoes of the same cross-track unit are located on the same straight line after RCMC, that is the curved hyperbola echoes have been corrected to a line. After RCMC and cross-track IFFT processing, the range-compressed 2-D echo can be obtained. In this case, the cross-track of echo is represented by the frequency f_r or the delay τ_r. Namely, the cross-track of the echo has become the sinc form response.

After the range compression, the echo needs RVP correction to remove the residual range migration. Then, the NsPE is corrected, which is named because this part of the error cannot be calculated in advance or expressed in analytical form. NsPE is mainly caused by nonsystematic motion, that is why we often call it motion error. The majority of motion errors can

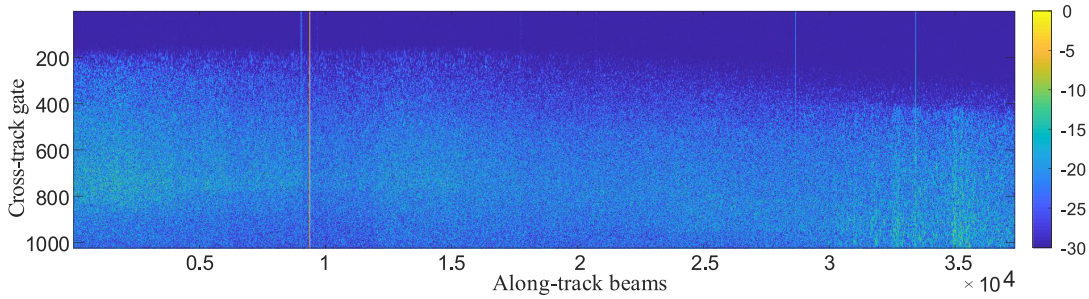

Fig. 5. 2-D rawdata echoes.

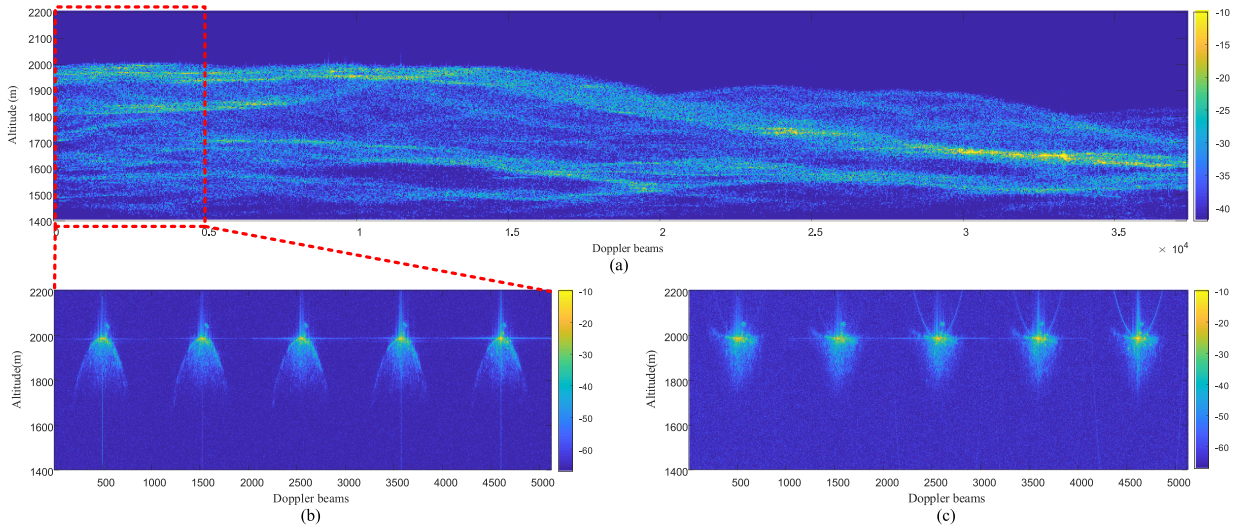

Fig. 6. Echoes of long along-track after range compressed and subaperture processing. (a) Echoes after range compression. (b) Echoes before RCMC of five subape.tures, (c) Echoes after RCMC of five subapertures.

be compensated by airborne inertial navigation, GPS, and other equipment. The NsPE here is the residual phase error after compensation by inertial navigation and other equipment. This residual NsPE will lead to defocus of echo data. Therefore, it is necessary to implement phase error estimation and compensation.

Next, in view of the classic and feasibility of PGA algorithm, the PGA is adopted to realize phase error estimation. According to the principle of PGA, it first realizes the phase gradient estimation of echo data, and then the phase error is calculated by the integrally step. The along-track overlapped subaperture PGA can accurately estimate the error phase of each subaperture, and then the phase error of the whole echo data can be obtained through the splicing step. To eliminate the gaps between phases estimated by adjacent sub-apertures, the splicing step is implemented in a half length overlap of along-track of a subaperture. The obtained phase error is shown in Fig. 8. Fig. 8(a) shows the result of phase error, the unit is radian, and Fig. 8(b) shows the motion error calculated by the phase error in (a). Note that the motion error refers to the movement distance of the onboard altimeter off course. It can be seen that the maximum phase error reaches about 680 rads, while the motion error does not exceed 6 m. Therefore, we can know that the flight of the airborne altimeter platform is relatively stable or that most of the motion errors have been compensated by the inertial navigation equipment. To this end, the phase error term is constructed by the obtained phase error in Fig. 8. By multiplying the phase error term to the echo after the RVP corrected, the NsPE is compensated.

For the convenience of the comparison of algorithms performance, we show the 2D-DDM results with and without PGA NsPE correction of one subaperture, which is show in Fig. 9. Due to the large size of along-track, a subaperture of the DDM is selected to show the performance of NsPE correction. It can be noticed that the DDM has a certain phase error in the Doppler beams before the NsPE correction, which leads to the defocus of the DDM in the along-track. After the PGA processing, DDM is focused obviously in the along-track, as shown in Fig. 9, which is beneficial to the improvement of the resolution in along-track. As shown in Fig. 10, the focusing result of dominant points with and without subaperture PGA treatment is obviously distinctive. It can be noted from Fig. 10 that the -3 dB bandwidth of the dominant scatter vertically below the airborne flight track is narrower than that without considering subaperture PGA, and the main lobe without PGA exists obvious spitting main-lobe. Moreover, the image entropy of with and without PGA for

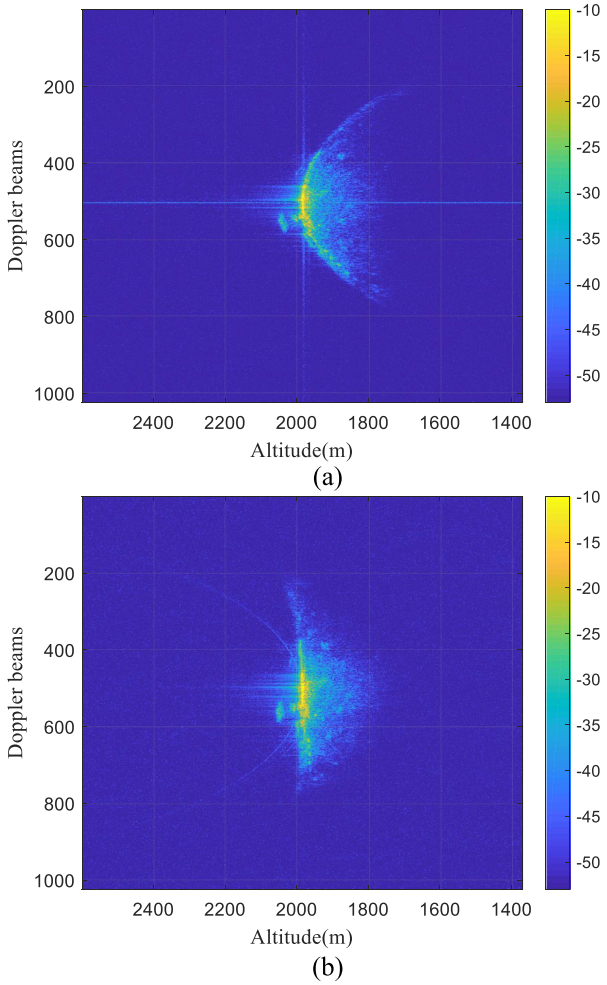

Fig. 7. Echoes of one subaperture before and after RCMC. (a) Echoes before RCMC, (b) Echoes after RCMC.

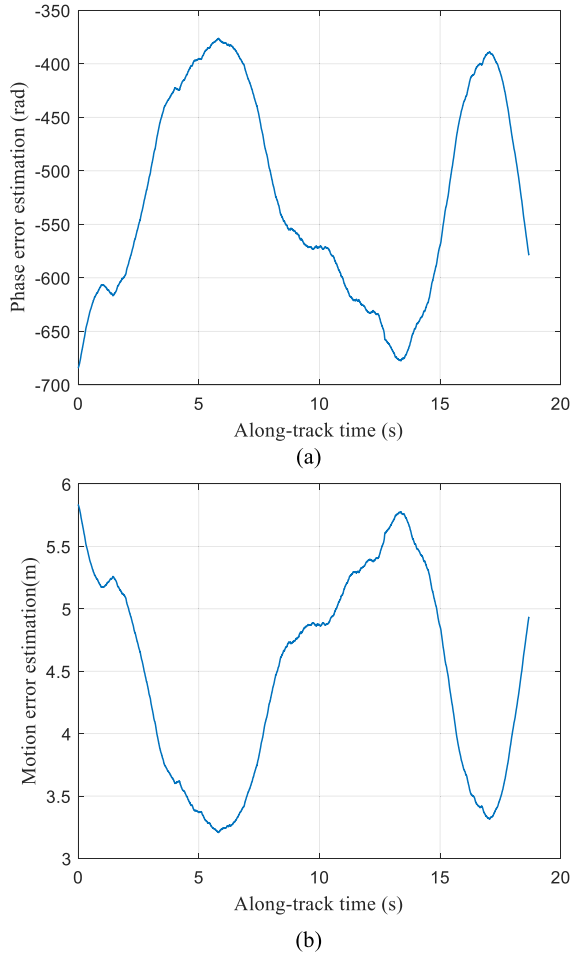

Fig. 8. NsPE estimation and motion error. (a) Nonsystematic phase error, (b) Nonsystematic motion error.

Fig. 9 are 9.7423 and 10.8050, respectively. Therefore, the proposed method is proved to be effective.

The echoes in each subaperture are implemented with coherent multilooking processing after subaperture PGA correction. The 1-D altimetry echoes are obtained as shown in Fig. 11, which is actually an expansion to three dimension of Fig. 9(b). During the long coherent processing, the raw data are divided into 72 subapertures, so that there are 72 echoes, and displayed in a 3-D graph in Fig. 11. The range gate of 1-D echo corresponding to each subaperture is closely related to the height delay, so it can be applied to retrack the ground scene altitude. In Fig. 11, the 1-D echo after multilooking represents the echo power. Since only the height delay parameter is retracked, the echo power will be normalized.

To this end, the 1-D echo can be retracked according to the procedure of Fig. 4. The Bayesian retracking algorithm takes the 1-D height echo as the observed signal, and prior of the altimeter delay parameter is designed as a flexible GGD. Under the assumption of Gaussian likelihood, the conditional posterior distribution of the delay parameter τ_r is obtained through hierarchical Bayesian and Bayesian inference, so that the statistical estimation model is constructed. On the other hand, 1-D altimetry echo needs to perform power normalization processing. Then, the retracking observation window needs to be selected, and initially match the theoretical convolution model, which is expected to achieve more accurate retracking. The matching result of the 1-D echo of a subaperture with the theoretical convolution model is shown in Fig. 12.

In Fig. 12, the number of range gates τ_r is proportional to the echo delay, and when the range resolution is known, the altitude information of the ground scene can be calculated through the range gate, which can be calculated as

$$\begin{aligned} h &= H_0 - (\tau_r + \tau_{st}) * \Delta r \\ &\approx H_0 - (\tau_r + \tau_{st}) * c/2B \end{aligned} \tag{40}$$

where H_0 denotes the height of altimeter platform, τ_{st} is the start gate number of observation window, and B is the bandwidth of transmitted LFM signal.

In Fig. 12, the theoretical convolution model achieves a good match with 1-D echo around the rising edge and peak, which RMSE is calculated as 0.0312. After the retracking of height parameter τ through the proposed Bayesian estimate algorithm, the altitude of ground can be obtained. In such cases, the flight

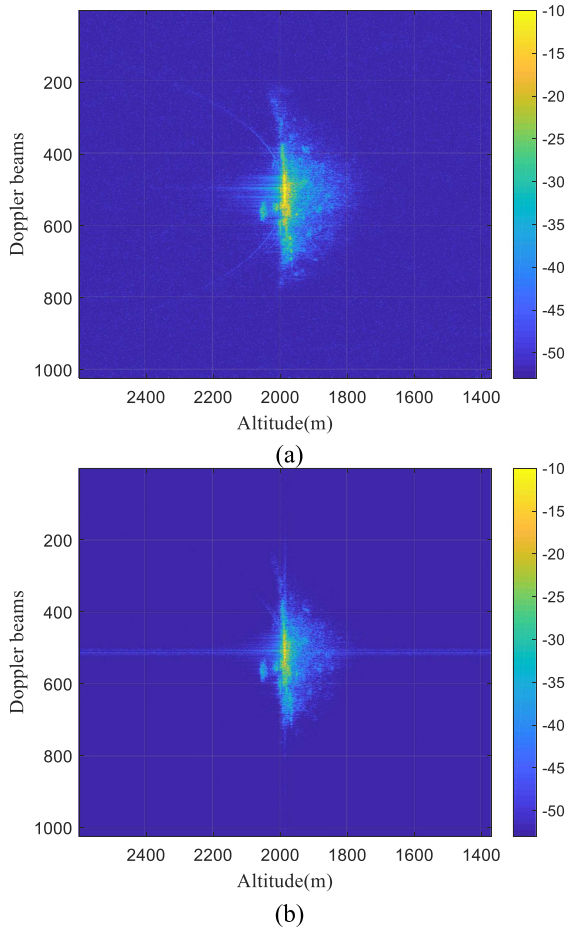

Fig. 9. Result of 2-D DDM of a subaperture with and without PGA nonsystematic phase error correction. (a) DDM without PGA correction, (b) DDM with PGA correction.

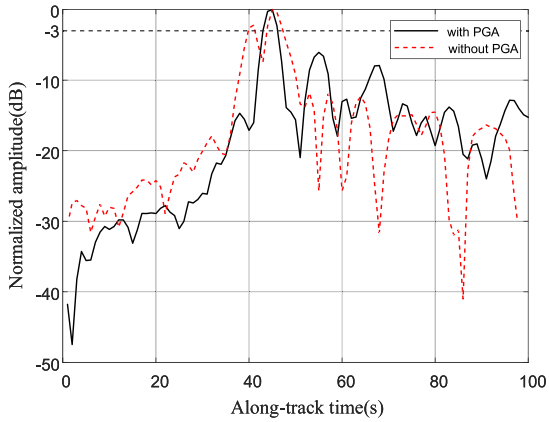

Fig. 10. Azimuthal response of a predominant scatter.

height of the airborne altimeter platform is 2600 m. According to the requirement of the altimeter in practice, the size of the observation window is set as 256 gate numbers, and the starting range gate is 400. The retracking height results of LS algorithm, MAP [13] algorithm and the proposed HMC algorithms are shown in Fig. 12.

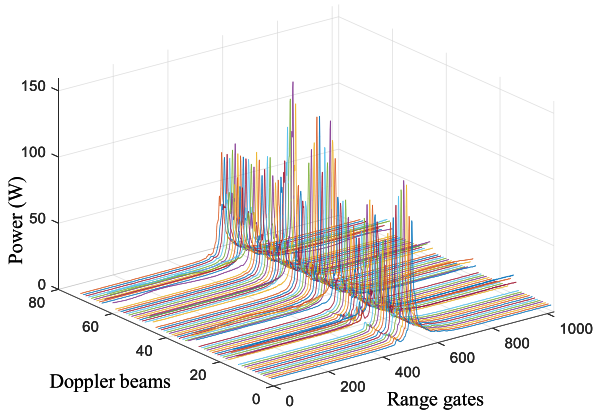

Fig. 11. Result of 1-D height echo in each subaperture.

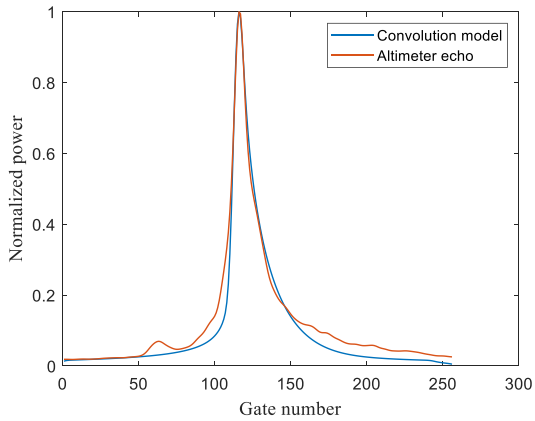

Fig. 12. Result of matching of 1-D altimetry echo and theoretical convolution model.

It can be noted from Fig. 13 that the altitude obtained by retracking is around 1980 m. The figure displays the ground truth of altitude and the altimetry results obtained by the three algorithms, where the ground truth is calculated by the range gate in the 3 dB power position with corrected by the GPS signal in the actual flight path. It is not difficult to find that the HMC algorithm has the highest tracking accuracy and it can always track the changing trend of altitude, followed by the MAP algorithm and the LS algorithm with the lowest tracking accuracy. The figure displays the reference of altitude [13] and the height results obtained by the three algorithms with the reference are calculated. The RMSEs of the LS, MAP, and HMC algorithms are 0.8367, 0.7516, and 0.6328, respectively. Therefore, the retracking results demonstrate the effectiveness of the proposed long-correlation processing and Bayesian height parameter retracking algorithm and its superiority over conventional algorithms.

VII. Discussions

From the theoretical analysis and experimental results in the above sections, it can be seen that a long CPI is capable of achieving a high-resolution in the along-track dimension for airborne

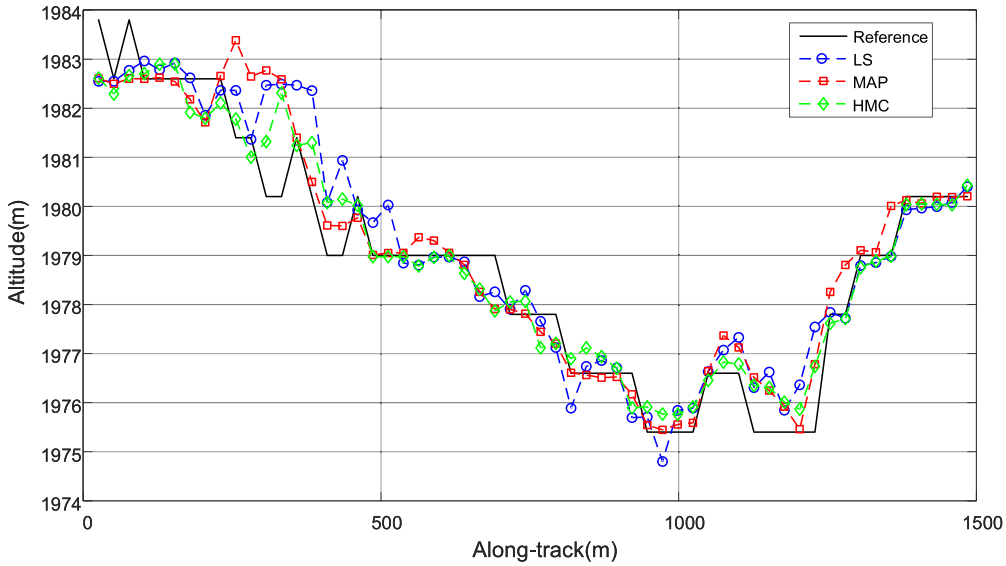

Fig. 13. Result of retracking for height parameter.

radar altimeter. However, the phase autofocusing is necessary in practice, which removes the defocus resulting from the airborne deviations due to atmosphere turbulence. Next, for an accurate height estimation, the Bayesian learning with a flexible prior achieves hierarchical formulation, and a closed-form solution for the posterior of the parameter estimation can be obtained. However, when the terrain is with multiple medium, which is out fitting of the Brown model, the height estimation would be invalid. This may need to resort to a power analysis method, and it will be discussed in our future work.

VIII. Conclusion

In this article, a novel long coherent processing interval SARAL altimetry algorithm based on Bayesian parameter retracking is proposed, which is used to solve the problem of the precision limitation of the conventional airborne SARAL altimetry. In the proposed algorithm, the subaperture delay correction processing and full-aperture coherent processing technology is utilized, which is expected to obtain the high-resolution DDM. The CPI of altimetry is synthetic aperture time, but not limited in the burst length. Considering the airborne SARAL is susceptible to turbulence, which results in defocus along-track. Therefore, a subaperture PGA framework is introduced. In this framework, the NsPE is estimated and compensated in along-track, which guarantees the resolution in along-track. In addition, since the traditional retracking algorithm is sensitive to noise, which affects the altimetry accuracy. Therefore, a Bayesian estimation method based on the HMC algorithm is proposed for retracking of SARAL, in which the echo prior is modeled as the GGD. Hence, the fully Bayesian estimation is obtained with the Bayesian retracking algorithm, and the altitude is estimated finally. The result of experiments verify the effectiveness and superiority of the proposed algorithm, and height parameter estimation of high resolution for SARAL is obtained via the proposed algorithm.

References

[1] R. K. Raney, "The delay/Doppler radar altimeter," *IEEE Trans. Geosci. Remote Sens.*, vol. 36, no. 5, pp. 1578–1588, Sep. 1998.

[2] A. Halimi, C. Mailhes, Jean-Yves Tourneret, P. Thibaut, and F. Boy, "A semi-analytical model for delay/Doppler altimetry and its estimation algorithm," *IEEE Trans. Geosci. Remote Sens.*, vol. 52, no. 7, pp. 4248–4258, Jul. 2014.

[3] P. C. Marth et al., "Prelaunch performance of the NASA altimeter for the TOPEX/poseidon project," *IEEE Trans. Geosci. Remote Sens.*, vol. 31, no. 2, pp. 315–332, Mar. 1993.

[4] L. Phalippou and V. Enjolras, "Re-tracking of SAR altimeter ocean power-waveforms and related accuracies of the retrieved sea surface height, significant wave height and wind speed," in *Proc. IEEE Int. Geosci. Remote Sens. Symp.*, 2007, pp. 3533–3536.

[5] A. Halimi, G. S. Buller, S. McLaughlin, and P. Honeine, "Denoising smooth signals using a Bayesian approach: Application to altimetry," *IEEE J. Sel. Topics Appl. Earth Observ. Remote Sens.*, vol. 10, no. 4, pp. 1278–1289, Apr. 2017.

[6] J. Chen and Y. U. Hanwen, "Wide-beam SAR autofocus based on blind resampling," *Sci. China Inf. Sci.*, vol. 66, no. 4, pp. 14, 2023.

[7] S. Zhou, L. Yang, L. Zhao, and G. Bi, "Quasi-polar-based FFBP algorithm for miniature UAV SAR imaging without navigational data," *IEEE Trans. Geosci. Remote Sens.*, vol. 55, no. 12, pp. 7053–7065, Dec. 2017.

[8] L. Yang, P. Li, S. Zhang, L. Zhao, S. Zhou, and M. Xing, "Cooperative multitask learning for sparsity-driven SAR imagery and nonsystematic error autocalibration," *IEEE Trans. Geosci. Remote Sens.*, vol. 58, no. 7, pp. 5132–5147, Jul. 2020.

[9] D. E. Wahl, P. H. Eichel, D. C. Ghiglia, and C. V. Jakowatz, "Phase gradient autofocus-a robust tool for high resolution SAR phase correction," *IEEE Trans. Aerosp. Electron. Syst.*, vol. 30, no. 3, pp. 827–835, Jul. 1994.

[10] S. Zhu, J. Yue, and W. Jiang, "SAS autofocus based on phase gradient autofocus," in *Proc. 4th Int. Workshop Chaos-Fractals Theories Appl.*, 2011, pp. 298–301.

[11] T. J. Kragh and A. A. Kharbouch, "Monotonic iterative algorithm for minimum-entropy autofocus," *Adaptive Sensor Array Process. Workshop*, vol. 40, no. 4, pp. 1147–1159, 2006.

[12] T. Zeng, R. Wang, and F. Li, "SAR image autofocus utilizing minimum-entropy criterion," *IEEE Geosci. Remote Sens. Lett.*, vol. 10, no. 6, pp. 1552–1556, Nov. 2013.

[13] A. Halimi, C. Mailhes, Jean-Yves Tourneret, and H. Snoussi, "Bayesian estimation of smooth altimetric parameters: Application to conventional and delay/Doppler altimetry," *IEEE Trans. Geosci. Remote Sens.*, vol. 54, no. 4, pp. 2207–2219, Apr. 2016.

[14] L. Shi, K. Xu, P. Liu, S. Yang, L. Wang, and X. Yu, "Height precision of SAR altimeter and conventional radar altimeter based on flight experimental data," *IEEE J. Sel. Topics Appl. Earth Observ. Remote Sens.*, vol. 9, no. 6, pp. 2676–2686, Jun. 2016.

[15] L. Yang, L. Zhao, G. Bi, and L. Zhang, "SAR ground moving target imaging algorithm based on parametric and dynamic sparse Bayesian learning," *IEEE Trans. Geosci. Remote Sens.*, vol. 54, no. 4, pp. 2254–2267, Apr. 2016.
[16] J. Chen et al., "Real-time processing of spaceborne SAR data with nonlinear trajectory based on variable PRF," *IEEE Trans. Geosci. Remote Sensing*, vol. 60, pp. 1–12, 2021.
[17] G. Brown, "The average impulse response of a rough surface and its applications," *IEEE Trans. Antennas Propag.*, vol. 25, no. 1, pp. 67–74, Jan. 1977.
[18] A. Egido and W. H. F. Smith, "Fully focused SAR altimetry: Theory and applications," *IEEE Trans. Geosci. Remote Sens.*, vol. 55, no. 1, pp. 392–406, Jan. 2017.
[19] L. Zhou, H. Yu, Y. Lan, and M. Xing, "Deep learning-based branch-cut method for inSAR two-dimensional phase unwrapping," *IEEE Trans. Geosci. Remote Sens.*, vol. 60, 2022, Art. no. 5209615.
[20] L. Chaari, Jean-Yves Tourneret, C. Chaux, and H. Batatia, "A Hamiltonian monte carlo method for non-smooth energy sampling," *IEEE Trans. Signal Process.*, vol. 64, no. 21, pp. 5585–5594, Nov. 2016.
[21] M. Pereyra, "Proximal Markov chain Monte Carlo algorithms," *Statist. Comput.*, vol. 26, pp. 745–760, 2016.

Cheng Fang received the B.E. degree in communication engineering from Jilin University, Changchun, China, in 2003, the M.E. degree in software engineering from Tianjin University, Tianjin, China, in 2011, and the Ph.D. degree in signal and information processing from the Department of Information Engineering, Beijing University of Posts and Telecommunications, Beijing, China, in 2017.

He has been working with the Tianjin Key Laboratory for Advanced Signal Processing, Civil Aviation University of China, Tianjin. His research interests include artificial intelligence computer vision, and Big Data analysis.

Ming Sun received the B.E. degree in communication engineering from Civil Aviation University of China, Tianjin, China, in 2022. She is currently working toward the M.E. degree in information and communication engineering with Tianjin Key Lab for Advanced Signal Processing, Civil Aviation University of China.

Her research interests include sparse Bayesian learning for SAR imaging and delay Doppler altimeter.

Bo Huang received the M.E. degree in measurement technology and instrument from University of Electronic Science and Technology of China, Chengdu, China, in 2011 and the Ph.D. degree in radio physics from China Academy of Engineering Physics, Beijing, China, in 2022.

He is currently working as an Associate Researcher and publishes more than ten papers in domestic and foreign journals and conferences since December 2022. He has been responsible for and participated in model development and pre-research projects of a number of national major weapons and equipment. His research interests mainly include radar altimeter system design, new radar detection technology research, and engineering application.

Fangheng Guan received the B.E. degree in automation from Hangzhou Dianzi University, Hangzhou, China, in 2021. He is currently working toward the M.E. degree with Civil Aviation University of China, Tianjin, China.

His research interests include SAR Image processing and artificial Intelligence.

Honghao Zhou received the B.E. degree in electrical engineering and automation from Civil Aviation University of China, Tianjin, China, in 2020. He is currently working toward the M.E. degree with Tianjin Key Lab for Advanced Signal Processing, Civil Aviation University of China.

His research interests include Airborne radar altimeter system and signal processing.

Xianhua Liao received the B.E. degree in electrical engineering and automation and the M.E. degree in electronics and communications engineering from Civil Aviation University of China, Tianjin, China, in 2017 and 2022, respectively.

He is currently as a mmwave radar engineer working with Shenzhen ChengTech Technology Co., Ltd, Shenzhen, China. His research interests include Bayesian learning for SAR imaging and automotive mmwave radar.

Lei Yang (Member, IEEE) was born in Tianjin, China, in 1984. He received the B.S. and Ph.D. degrees both from Xidian University, Xi'an, China, in electronic engineering and signal and information processing, in 2007 and 2012, respectively,.

From 2012 to 2017, he was with the School of Electrical and Electronic Engineering, Nanyang Technological University (NTU) and Temasek Lab @ NTU, Singapore, as a full-time postdoctoral research fellow and Research Scientist, respectively. He is currently working with Tianjin Key Lab for Advanced Signal Processing, Civil Aviation University of China as a Full Professor. His research interests mainly include high-resolution radar imaging and implementation, machine learning for SAR imaging, etc.